

Highlights

- Thermal stability and fire behaviour of polyisocyanurate insulation foams with smart fillers
- Such fillers are Layered Double Hydroxides, Expandable Graphite and Ammonium Polyphosphate
- Cone calorimeter data showed that fillers addition decreased heat release rate
- Thermogravimetric analysis coupled with FTIR were used to determine different pyrolysis gases
- Post-burning residuals and morphological evaluation supported the beneficial addition of fillers

1 **Effect of Layered Double Hydroxide, Expanded Graphite and**
2 **Ammonium Polyphosphate additives on thermal stability and fire**
3 **performance of polyisocyanurate insulation foam**

4

5

6 **Abstract:**

7 This work examines the effect of Layered Double Hydroxides (LDHs), Expandable Graphite (EG)
8 and Ammonium Polyphosphate (APP) on the thermal stability and behaviour under fire conditions
9 of polyisocyanurate (PIR) insulation foams. Virgin materials' and char residues' morphologies
10 were analyzed with a variety of experimental techniques including field emission scanning
11 electron and optical microscopy along with Raman spectroscopy. Thermal stability and burning
12 behaviour were examined using thermogravimetric (TGA) coupled with Fourier Transform
13 Infrared (FTIR) spectrometer and cone calorimeter. TGA results suggested a decrease in
14 degradation temperature upon introduction of fillers in PIR samples. FTIR spectra were used to
15 determine the absorbance intensity of the different pyrolysis gases. Cone calorimeter data analysis
16 established a limited effect on reducing the rate of heat release rate and smoke production with the
17 inclusion of LDHs. However, EG or EG+APP addition, caused a considerable decrease in heat
18 release rate, owing to the increased char strength and the release of non-combustible gases. The
19 positive effect of EG or EG+APP in the fire behaviour of PIR foams was further supported by the
20 morphological evaluation of their residual char samples.

21

22

23 **Keywords:** thermal stability; fire performance; polyisocyanurate insulation foams; Layered
24 Double Hydroxides; Expanded Graphite; Ammonium Polyphosphate.

25

26 **1 Introduction**

27 A worldwide roll-out of near-Zero Energy Buildings drives the design of exterior wall systems
28 with the purpose of achieving building sustainability and high energy efficiency. Energy efficient
29 insulation materials usage in building envelopes is identified as the main practice, that can actively
30 contribute towards achieving greenhouse gases emissions targets and energy consumption
31 reductions [1, 2]. Recent advantages in the development of insulation materials have promoted the
32 use of different types of insulations techniques for external walls. Currently, there is a wide range
33 of insulation options comprising of non-combustible, limited combustible or combustible
34 materials. Most commonly used foams, with or without flame retardants, in the family of
35 polymeric insulation materials include extruded and expanded polystyrene, polyurethane foam
36 (PUF) and polyisocyanurate (PIR) [3]. These inherently combustible and highly insulating
37 materials are extensively used in most construction sectors for their high energy performance and
38 cost benefit but should be designed not to compromise their fire safety.

39 Recent studies on polymeric foams [e.g., 3-5] have established that their thermal decomposition
40 consists of numerous decomposition pathways that mainly depend on their organic compound
41 reactivity. Specifically, PIR consist of diisocyanates or prepolymers that form ring structures, also
42 referred to as isocyanurate rings [6]. From a thermodynamic point of view, PIR materials are thus
43 considered superior to PURs as they are more thermally stable compared to urethane bonds found
44 in PUR foams. The thermal stability of PIR is demonstrated by the fact that they dissociate at
45 higher temperatures at the range of 350 °C as opposed to 200 °C observed for urethanes [7].
46 Therefore, understanding how the use of reactive or additive flame retardants can modify, reduce,
47 delay or even stop their combustion [3-12] is attracting considerable scientific interest.

48 To further promote sustainable practices in the construction sector, a growing body of study has
49 been lately devoted to examining the potential of substituting popular halogen-based flame
50 retardants with second-generation eco-friendly substitutes. The study of eco-friendly flame
51 retardants such as Layered Double Hydroxides (LDHs) [4, 5], is of great interest as they are found
52 to increase the flame retardancy and thermal stability in polymers by suppressing smoke and
53 reducing the release of volatile compounds [8]. The benefits of using them also derives from the
54 fact that they may act in both gas and solid phases during polymer combustion. Non-flammable

55 gases, including water and carbon dioxide, that are released during their combustion can further
56 dilute flammable gases, thus reducing endothermic decomposition of metal hydroxides and
57 promote surface charring of polymers.

58 The use of different binary and ternary LDHs in various polymeric insulating materials has been
59 investigated by numerous authors; those LDHs include ZnAl and MgAl carbonates, MgAl stearate
60 and ZrP with contents, ranging from 0.2% to 6%, [4, 5, 9]. Despite their effectiveness, LDHs up
61 to now have not met commercial success due to the inherent difficulty to uniformly disperse and
62 distribution in polymers, [4]. Whilst so far, most studies [4, 5, 8] were concerned with fire
63 retardancy effects of LDHs on PUF, recent studies [9, 10, 11] investigated the effect of lamellar
64 inorganic [9] and organic LDHs [11] on flame retardancy of PIR. It has been demonstrated that
65 lamellar inorganic LDHs [9] enhanced the fire retardancy of PIR as initial degradation temperature
66 was increased, degradation was decelerated, and significant char formation was observed.
67 Improved char properties and decreased heat release was also observed when increasing filler's
68 content. Organically modified nanoclay LDHs [11] improved flame retardancy and stability of
69 rosin based PIR foam and showed synergistic effect with other flame retardants. During the
70 combustion process, some of the most efficient LDHs proved to be the Expanded Graphite (EG)
71 and Diethyl Ethylphosphonate. The reason was LDHs' promotion of a reinforced char layer that
72 could provide a more effective thermal barrier against heat and oxygen as well as more effective
73 suppression of smoke and flammable gases.

74 The synergistic effect of LDHs and other flame retardants, such as EG or Ammonium
75 Polyphosphate (APP), were further investigated [11-17] and recent evidence revealed that the fire
76 behavior of PIR [10, 18] and PUR [19, 20] foams can be substantially improved. This was
77 attributed to the fact that, EG is a graphite intercalation compound with a special layered structure,
78 which is found to expand when exposed to heat forming a huge insulation layer that can further
79 enhance PIR fire resistance [11, 21]. EG having a boiling point above 3000 °C is able to maintain
80 its integrity as it mainly acts in the condensed phase both in terms of smoke suppression and
81 insulation [19]. This insulation char layer is characterized by a "worm-like" appearance which,
82 results from the expansion of H₂SO₄ that is intercalated between graphite layers and the release of
83 CO₂, H₂O and SO₂ gases [22, 23]. APP consists of a high molecular weight polyphosphate chain
84 and it mainly acts in the condensed phase by contributing to increased char formation [19, 21].

85 Furthermore, studies revealed that APP and EG can further improve char formation due to the
86 synergy of the phosphoric acid with graphite [19, 22].

87 Despite previous extensive research on the flammability of PIR and PUR foams [4-12, 18-23], few
88 researchers [11, 18] have investigated the interaction of LDHs with nanometric particles and
89 phosphorous based materials in PIR foams and how they affect their flame retardancy. Therefore,
90 this work aims to extend existing work on polymer flammability [4, 5, 6, 7, 9] and specifically,
91 experimentally investigate the thermal stability and fire behavior of PIR foams containing a range
92 of lamellar inorganic smart fillers, namely LDHs, EG and APP. Emphasis is given on the
93 interaction of LDHs with both APP and EG and how their synergy is contributing towards
94 improved PIR foam flame retardancy. Fire properties and thermal stability of the samples were
95 assessed using cone calorimetry and thermogravimetry techniques coupled with FTIR
96 spectrometry. Virgin materials and char residues morphology was analyzed with a variety of
97 experimental techniques including field emission scanning electron and optical microscopy along
98 with Raman spectroscopy. Post-burning and cellular morphology characterization of the residual
99 materials was also conducted using both field emission scanning microscopy and Raman analysis.

100

101 **2 Experimental investigation**

102 **2.1 Preparation of materials**

103 PIR samples with an isocyanate index (NCO/OH) of 3.0 were produced at SELENA Labs as
104 described in the previous authors' work [9, 10]. Main components of the samples, including the
105 polyol, the catalysts, the stabilizer and blowing agent (methylal), were initially premixed for up to
106 3 minutes at 1500 rpm. Polyol blend components' viscosity at 25 °C was measured below 500
107 mPa·s and below 260 mPa·s for isocyanate. Fillers were then added to the mix of each different
108 sample and all PIR samples were further mixed for 5 min at 2500 rpm. All fillers used, i.e., Layered
109 Double Hydroxides containing MgAlCO₃ (LDH), Expanded Graphite (EG) and Ammonium
110 Polyphosphate with high (APP1) and low degree of polymerization (APP2); final formulations
111 were prepared at SELENA Labs. In more details, EG, provided by Asbury Graphite Mills Inc., has
112 a nominal size greater than 75 μm and Carbon content above 80 % w/w, Sulfur above 3 % w/w

113 and an expansion ratio of 60:1 cc/g. Carbonate form of MgAl LDH, $Mg_4Al_2(OH)_{12}(CO_3) \cdot 6H_2O$,
114 was supplied by Prolabin and Tefarm Srl. Due to its layered structure it is easily employed as an
115 active filler able to improve the efficacy of the main PIR formulation. Ammonium Polyphosphate,
116 NH_4PO_3 with high degree of polymerisation (APP1), (average degree of polymerisation $n > 1000$),
117 was used in crystal phase II. It is largely insoluble in water and completely insoluble in organic
118 solvents containing 31-32 % w/w Phosphorus and 14-15 % w/w Nitrogen. APP1 was provided by
119 Clariant Produkte GmbH. It is colourless, non-hygroscopic and non-flammable. It is suitable as a
120 non-halogenated flame retardant for polyurethane foams. It is also biodegradable as it breaks down
121 to naturally occurring phosphate and ammonia with decomposition temperature above 275 °C. It
122 has a high heat stability, however to prevent APP1 from settling, it was stirred into the mixture.
123 Ammonium Polyphosphate, NH_4PO_3 with low degree of polymerisation (APP2), $n > 50$, was used
124 in crystal phase I and supplied by Shandong Chenxu New Material Co. Ltd. P_2O_5 content was
125 above 69 % w/w and Nitrogen above 13 % w/w.

126 In total, four formulations were examined, and their fire performance was evaluated against plain
127 PIR samples (REF). Research on LDH and APP additives in PIR revealed that their incorporation
128 in polyurethane composites in a range of concentrations from 0.5 % to 8 %, improved their thermal
129 properties flame retardancy resulting in a decreased HRR [9]. Three different concentration of
130 LDH have been studied, namely 2 %, 4 % and 6 % and the research group decided to use 2 % LDH
131 in order to secure both low price and high efficiency-to-price ratio. EG and APP concentrations
132 were chosen according to scientific literature [11, 12, 13, 18, 20], suppliers' recommendations and
133 our research group previous experience [9, 10]. In that respect, three different formulae flame
134 retardants were used: the first set contained $MgAlCO_3$ at 2 % wt (PL), the second one contained
135 additionally 5.1 % wt EG (PLE) and the third set contained 3.6 % wt APP1 (PLEAPP1) or 3.6 %
136 wt APP2 (PLEAPP2) as depicted in Table 1. The physical and mechanical characteristics of all
137 the samples are presented in Table 1, namely, density, average cell diameter, closed cell
138 percentage, thermal conductivity, compressive strength and tensile strength.

139

140 2.2 Test methods

141 2.2.1 Morphology and cellular structure

142 Morphological evaluation of PIR foam samples was conducted at 500 μm with the use of optical
143 microscopy. To provide elemental identification, virgin and charred PIR samples cell structure
144 was further investigated using a field emission scanning electron microscopy (FESEM, Hitachi
145 SU 5000) at 15 kV accelerating voltage. Raman characterization was also used to assess the quality
146 and uniformity of residual chars using an excitation wavelength of 532 nm (RL532C laser source)
147 at a Renishaw Invia Qontor system.

148

149 2.2.2 TGA - FTIR

150 Thermogravimetric analysis (TGA) was performed on a Mettler Toledo instrument under both
151 reactive (air) and inert (N_2) atmosphere from 20 $^\circ\text{C}$ to 700 $^\circ\text{C}$ at a heating rate of 20 $^\circ\text{C}/\text{min}$ with
152 sample sizes of 10 ± 1 mg in an no lid aluminum sample cup at a 150 ml/min gas flow. Thermal
153 stability was evaluated by determining for each sample the initial degradation temperature
154 corresponding at 5% weight loss ($T_{5\%}$), the weight (W_i) and corresponding temperature ($T_{max,i}$) at
155 the maximum weight loss rate of each degradation step (i) and the percentage of the char residue
156 at a temperature of 700 $^\circ\text{C}$. A Bruker Tensor 27 FTIR spectrometer was coupled with the TGA
157 apparatus to analyze the gaseous emission released real time during each TGA test. Each infrared
158 spectrum was recorded in a wavenumber range of 4000–740 cm^{-1} using 1.0 cm^{-1} spectral resolution
159 and 64 scans. Results were analyzed using OPUS 8.2 spectroscopy software.

160

161 2.2.3 Cone calorimeter

162 Cone calorimeter (CC) tests were performed according to the ISO 5660-1 [24], utilizing a Dark
163 Star Research Ltd (UK) apparatus. The samples sizes were 100 mm x 100 mm x 24 mm and were
164 horizontally placed in a stainless-steel metal holder. The back and sides of the sample were
165 insulated with 2 sheets of 3 mm thick high temperature vitreous wool Insulfrax[®] Paper having a

166 nominal density of 150 kg/m^3 and conductivity 0.098 W/mK at $400 \text{ }^\circ\text{C}$, coated with 0.07 mm
167 AT502 30 Micron aluminum foil tape, Category 1 according to BS476 Part 6 and 7 [25, 26]. All
168 samples were conditioned before testing according to ISO 554 [27] at $23^\circ\text{C} \pm 2 \text{ }^\circ\text{C}$ at $50 \% \pm 5$
169 $\%$ relative humidity. The tests were repeated at least twice for each formulation to check
170 reproducibility. To avoid preheating effects, the surface of each sample was carefully insulated
171 before exposure to heat. The following parameters were investigated for each sample: time to
172 ignition (TTI); Combustion Time (CT); Total HRR (THR); peak HRR (p-HRR); average HRR
173 (Av-HRR); average mass loss rate (Av-MLR), smoke production rate (SPR); smoke and CO yield.
174 Specimen burning and smoke color observations were recorded by positioning two digital cameras
175 facing and sideways of the test apparatus. Two heat flux levels were used to examine the fire
176 performance of the samples at both low (20 kW/m^2) and high (50 kW/m^2) heat fluxes. The
177 uncertainty of the measurements conformed to ISO 5660 [28].

178

179 **2.2.4 Thermal conductivity**

180 Plane Source method was used to measure the sample's thermal conductivity in accordance to ISO
181 22007-2 [29] at $10 \text{ }^\circ\text{C}$ was reduced from 31.5 mW/mK for neat PIR to 25.6 mW/mK and 24.8
182 mW/mK for PLEAPP1 and PLEAPP2 samples respectively, Table 1.

183

184 **3 Results and discussion**

185 **3.1 Optical Microscopy and FE-SEM**

186 Optical microscopy and FE-SEM, Figures 1 and 2, were used to evaluate the morphology and
187 cellular structure for selected PIR formulations. Figure 1 shows that LDHs do not significantly
188 alter the morphology of the PIR samples. The FE-SEM results indicate that the average cell
189 diameters of REF, PL, PLE, PLEAPP1 and PLEAPP2 samples are presented in Table 1. A slight
190 decrease in the average cell diameter with fillers addition was observed.

191

192 3.2 Thermogravimetric analysis and gas phase flame retardancy

193 Combined FTIR/TGA analysis was used to understand the pyrolysis of the PIR samples by
194 identifying the gases evolved at different stages of their pyrolysis. Figures 3 and 4 present the
195 weight and derived weight loss rate of all samples under N₂ and Air atmospheres respectively. A
196 summary of the results is provided in Table 2. TGA analysis revealed that degradation temperature
197 of filler layered PIR samples decreases, when compared to the virgin PIR samples (REF). PIR
198 samples containing APP degrade in two steps, under both inert and reactive atmospheres. Those
199 two steps are associated with the degradation of the hard segment urethane-urea linkages and of
200 the polyol derived products from isocyanurate. During those processes low calorific combustion
201 products are initially released during the first degradation step and later higher calorific
202 combustion products are produced due to the polyol derived products of the second degradation
203 step. With the addition of APP, an additional degradation step was observed at around 530 °C
204 associated with the degradation of APP. Combination of such phosphorus containing additives,
205 e.g. APP, with LDHs has been shown to improve the additives dispersion within the polymer mix.
206 A major advantage of their combination is also the observed reduction in the overall additive
207 concentration required to achieve satisfactory flame-retardant properties in thermoplastics [30].
208 The initial degradation temperature, $T_{5\%}$, is 258 °C for pure PIR. $T_{5\%}$ decreases slightly with the
209 addition of LDH compared to neat PIR foam, whereas much more substantially EG-containing
210 formulations (w/wo APP). The first pyrolysis step observed in between 200 °C and 400 °C, is
211 identified as the primary mass loss step [31, 32].

212 The temperature at the maximum degradation rate, $T_{max,1}$, is slightly decreased with the LDH filler,
213 whereas it is substantially decreased with the incorporation of EG or EG with APP. This behaviour
214 is owed to the degradation of the hard segment [33] and the residual weight of this first reaction is
215 denoted as W_1 . The degradation of the polyol derived products, second decomposition stage,
216 resulted in lower residual weight denoted as W_2 and was observed between 400 °C and 600 °C.
217 Maximum degradation temperature during this step, $T_{max,2}$, is 457 °C and residue mass, 25.4 %
218 were observed for PIR samples under air atmosphere. EG addition resulted in $T_{max,2}$ and mass
219 residue decrease due to fillers degradation at lower temperatures. The former decrease is more
220 substantial with the addition of EG and APP [13, 14, 15]. It is also important to note that the final
221 residue of APP containing formulations is significantly higher than that of other formulations,

222 indicating that APP is a very effective charring agent. Results are in line with earlier findings from
223 the literature [30, 34, 35] indicating that APP additives decompose at elevated temperatures and
224 produce phosphoric and polyphosphoric acids. Those acids are known to promote charring via
225 formation of reactive polymer fragments cross-linkages that prevent or slow down heat transfer.
226 Oxygen and combustible volatiles cannot easily transfer into the pyrolysis zone due the formation
227 of this carbonized char network. The combination of EG, LDH and APP results in a third
228 degradation step after 500 °C. Addition of EG and LDH with APP serves to reduce
229 depolymerization and enhanced char formation perhaps due to synergistic interactions [30]. For
230 samples PLEAPP1 and PLEAPP2 the final residue is about 37 % in both atmospheres.

231 Gaseous emissions FTIR spectrums are displayed in Figure 5 for all samples in both atmospheres
232 and at various temperatures. The characteristic bands of degradation of pure PIR can be identified
233 as hydrocarbons (3000-2850 cm^{-1}), aromatic compounds (1638 cm^{-1}), CO_2 (2400-2300 cm^{-1}), -
234 NCO compounds (2300-2200 cm^{-1}), CO (2181 cm^{-1}) and ethers (1153 cm^{-1}). The degradation of
235 the polymer polyol and urethane is visible in the changes of the spectra between 1000-1500 cm^{-1}
236 wavelengths, clearer under N_2 atmosphere, consistent to the literature [33]. PIR samples containing
237 EG, APP1 And APP2 release similar pyrolysis products to pure PIR samples.

238 Utilising the FTIR spectra, we performed integration over specific wavenumber ranges and
239 determine the absorbance intensity of the different pyrolysis gases. Figure 6 demonstrates a
240 comparison of the absorbance of ethers, -NCO, CO and CO_2 over time for all samples in air. CO
241 was detected between 200 °C and 650 °C with a maximum value at 500 °C, under air atmosphere
242 and from 100 °C to 1000 °C with a second maximum value at 950 °C for samples containing APP1
243 and APP2 under inert atmosphere. Carbon dioxide emissions show one peak between 350 °C and
244 700 °C with a maximal value at 600 °C under inert atmosphere. Two peaks are observed under air
245 atmosphere and the maximal values are recorded at a lower temperature of 500 °C. Gaseous
246 emissions pattern detected in this work are consistent with previous results [5-7, 36] regarding the
247 thermal degradation and carbonization performance of PIR with different fire-retardant fillers.

248

249 **3.3 Cone calorimetry**

250 HRR and SPR histories of all formulations at 20 kW/m² and 50 kW/m² are depicted in Figures 7
251 and 8. It is worth noting that all formulations (except PLEAPP1 at 20 kW/m²) ignited almost
252 immediately after being exposed to the heat source, due to their low density and high flammability.
253 Neat PIR has the highest HRR and SPR as expected. Fissures were observed on the final char
254 residue at the end of the test along with detachment and exfoliation of the upper layer surface as
255 highlighted in Table 3. The trends of SPR are similar to those of HRR, and consequently we will
256 focus our discussions on the HRR. With the addition of LDH alone, there is a small decrease in
257 the first HRR peak with a more substantial reduction in the second HRR peak. The char also
258 appears stronger than that of the neat PIR. APP addition to PIR samples resulted in lower PHRR
259 values or no ignition at the lower heat flux. Simultaneous presence of LDH and APP in PIR
260 samples can successfully promote char formation. This concurs well with previous research on
261 chemical interaction of APP and LDH in polystyrene [30]. With a further inclusion of EG, the
262 HRR is reduced further, however, it is interesting to note that APP2 has limited effect on the HRR
263 compared to EG alone, whereas PLEAPP1 achieves the lowest HRR and SPR, most likely because
264 of the increased strength of the char layer as shown in Table 3. This strengthened char layer
265 provides a resilient barrier, preventing heat and oxygen penetration to the material and release of
266 non-combustible gases. At the same time, it can effectively suppress smoke and gases during the
267 combustion process. The present results demonstrate that the degree of polymerization has a very
268 important effect on the fire retardancy of the composites as shown in both Figures 7, 8 and Table
269 3.

270 Another important finding is that LDH decreases smoke and CO yields compared to neat PIR
271 (REF). Improved fire behaviour when EG and APP2 fillers are used, is evident as the flame-
272 retardant properties of PLEAPP2 sample are improved significantly. Both the p-HRR and Av-
273 HOC are decreased with additions of fillers. EG having considerably lower values of heat of
274 combustion than REF or PL confirms that it also acts in the gaseous phase in suppressing
275 combustion [17]. One other important observation is that all the fillers have either similar or lower
276 smoke or CO yields compared to neat PIR, highlighting one of their main advantages of these type
277 of fire retardants in comparison to halogenated fire retardants.

278

279 **3.4 SEM and Raman residual char characterization**

280 Figure 9 presents the char residue of all samples after CC testing under both heat fluxes. Fillers
281 were found to promote the formation of more rigid and hardened residual char layer. In virgin PIR
282 samples, the char was brittle and non-uniformly distributed. In addition, detachment and
283 exfoliation of the upper layer surface was also observed. A clear difference in appearance was
284 observed in the residual char for PLEAPP1 and PLEAPP2, which were intact and spongy. Clearly,
285 the strength and integrity of the char plays a very important role in reducing the burning rate/heat
286 release rate for meso- to large-scale samples, in which internal heat and mass transfer becomes
287 important, as opposed to the mg samples used in TGA. Plain PIR char residues show a looser
288 structure, which indicates inefficient barrier protection for underlying layers. PL char residue was
289 more coherent. The addition of EG resulted in a more compact char structure although minor
290 cracks in the surface could still be observed. Comparing to the rest of the char residue
291 morphologies, the char residues PLEAPP1 samples were more compact than the rest of the samples
292 and no cracks appeared on the surface.

293 Char residues were further evaluated in terms of field mission SEM analysis to explore the specific
294 mechanisms. Char samples investigated were taken after performing CC at high heat flux of 50
295 kW/m². In Figure 10 (a)-(c), it can be observed that cells were severely broken, and an open cell
296 polyhedral structure was dominant in virgin PIR samples. With the addition of 2 % LDH, Figure
297 10 (d)-(f), PL sample's cellular structure became loose and permeable and this was an indication
298 that the flame shield created was not as strong. Numerous bright amorphous regions scattered
299 across the image are identified as residual fillers. In the rest of the samples containing EG, Figure
300 10 (g)-(h), (j)-(k), (m)-(n), "worm-like" char regions are observed and scattered throughout their
301 porous sheeted structure as also reported in [37]. The addition of APP1 and APP2 results in a
302 tighter and denser morphology than the materials added with only expandable graphite, in
303 accordance to previous studies [38]. The fact that the combination of APP, EG and LDH can
304 promote the formation of an intumescent residue with superior barrier properties compared to
305 samples containing only APP is likely due to the combination of a reduced heat and mass transfer
306 due to intumescence and reduced permeability of the residue [30].

307 The graphitic structure of PLE, PLEAPP1 and PLEAPP2 char residue samples was investigated
308 with Raman spectroscopy, Figure 11. The G peak at 1580 cm^{-1} corresponds to vibrations of in
309 plane sp^2 carbon atoms in graphite. The D peak at 1350 cm^{-1} is associated with the vibration of
310 carbon atoms in disordered graphitic structures [38]. The graphitized structure, acts as a physical
311 barrier and is an indication of increased thermal stability. D and G intensity band ratio (I_D/I_G) was
312 utilized for estimating the degree of graphitization in residual char; a higher degree of
313 graphitization is associated with decreased I_D/I_G values [39]. PLE sample exhibited the lowest
314 I_D/I_G value of 0.12, hence the highest degree of graphitization, followed by samples PLEAPP1 and
315 PLEAPP2, which exhibited values of 0.40 and 0.48 respectively.

316

317 **4 Flame retardant mechanism of LDH, EG and APP additives on flame retardancy**

318 Figure 12 represents the proposed mechanism of LDH, EG and APP additives on flame retardancy
319 of PIR. APP, EG and LDH can promote the formation of an intumescent residue with superior
320 barrier properties [10, 12, 13, 14, 15, 17]. It is attributed to the combination of a reduced mass and
321 heat transfer mechanism, due to reduced permeability residue and intumescent [12].

322 As it is depicted, the existence of a resilient char layer is crucial for guarantying the flame
323 retardancy of the underlying PIR matrix. Cone calorimetry and thermogravimetric analysis
324 revealed that a strong char layer can prevent penetration of heat and oxygen and thus reducing PIR
325 thermal degradation, decreasing HRR and pyrolysis gas release. Formation of a resilient char layer
326 also shields the rest of the sample underneath it from radiation. The diffusive gases navigate around
327 LDH and APP nanofillers that act as barriers preventing pyrolysis gases to move towards the
328 exposed surface. APP was found to act in the condensed phase and acts in a beneficial way as it
329 promotes sample dehydration and carbon-forming.

330 During thermal decomposition, LDH fillers lose the interlayer water. The decomposition of the
331 intercalated anions and metal hydroxide produces water vapor and gases, e.g. CO_2 , which
332 eventually reduce the availability of combustible fuel vapors resulting in decreased heat release
333 and promotion of char formation.

334 Cone calorimetry revealed that smoke and CO yields values of all formulations containing LDH,
335 APP and EG are similar, lower than those of virgin PIR. This is a strong indication that neither of
336 the fillers promote pyrolysis gases production. It can also be speculated that the samples containing
337 APP were more cohesive and formed more compact char layer. Intumescence of the char in
338 PLEAPP1 and PLEAPP2 samples is stabilized and improved as the right proportion of LDH
339 crosslink with APP; further to that, they present increased viscosity due to higher molecular weight
340 APP and the presence of EG. The fact that samples containing EG have considerably lower values
341 of heat of combustion than REF or PL samples confirms that EG also acts in the gaseous phase in
342 accordance to bibliography [17].

343

344 **5 Conclusions**

345 Fire-reaction properties and thermal stability of PIR form with smart fillers including LDHs, EG
346 and APPs were evaluated using thermogravimetry and cone calorimetry. Optical microscopy and
347 scanning electron microscopy measurements were also performed for the samples, which verified
348 that the fillers were exfoliated in the PIR samples. Post-burning characterization and
349 morphological assessment of the residual materials revealed that all fillers stimulate the formation
350 of a reinforced char layer. LDHs alone have limited effect on reducing the HRR or SPR since they
351 only act in the solid phase. With the addition of EG or EG+APP, the HRR is further decreased
352 owing to the increased char strength as well as the release of non-combustible gases that during
353 combustion adequately suppress smoke and gases production. There are strong indications that
354 additives studied in this work can effectively slow down or even prevent depolymerization of PIR
355 and simultaneously promote char formation. The best performance was achieved by PLEAPP1
356 with high degree of polymerization that resulted in resilient char formation, decreased heat release
357 values, smoke generation and CO production. This result confirms that the degree of
358 polymerization of fire retardants is significant in its fire performance.

359 The present results clearly indicate that the use of smart fillers (LDH, EG and APP) in PIR foams
360 can significantly increase their thermal stability and fire behaviour, which is of great importance
361 in the development of safe and highly efficient insulation products that can be used in the building
362 industry, and especially in cost-effective building envelopes in order to bring opaque components

363 of curtain wall building systems to “nearly zero energy” standards. Whilst we used only small-
364 scale samples in this work, it is worth noting that preliminary tests of selected formulations in
365 single-burning-item (SBI) have been carried out with promising results. Further assessment of the
366 fire performance of the foams incorporated into a complete façade system will also be conducted
367 in furnace tests in the near future.

368 **6 Acknowledgements**

369 This work was financially supported by the EENSULATE H2020 project (EEB-01-2016, Grant
370 No. 723868).

371

372 **7 References**

373 [1] UN Environment and International Energy Agency 2017: Towards a zero-emission, efficient,
374 and resilient buildings and construction sector. Global Status Report 2017.

375 [2] Directive 2018/844/EU of the European Parliament and of the Council of 30 May 2018
376 amending Directive 2010/31/EU on the energy performance of buildings and Directive 2012/27/Eu
377 on energy efficiency. Off. J. Eur. Union 2018, 156, 75–91.

378 [3] D. O’Connor, The Building Envelope: Fire Spread, Construction Features and Loss Examples,
379 SFPE Handbook of Fire Protection Engineering (5th ed) Hurley M.J. (ed.), National Fire Protection
380 Association, Quincy, MA 02269, 2016, p 3242/3512.

381 [4] Y.C. Li, Y.H. Yang, J.R. Shields, R.D. Davis, Layered double hydroxide-based fire-resistant
382 coatings for flexible polyurethane foam, *Polymer* 56 (2015) 284-292,
383 <https://doi.org/10.1016/j.polymer.2014.11.023>

384 [5] S. Gomez-Fernandez, L. Ugarte, C. Pena-Rodriguez, M. Zubitur, M.A. Corceuera, A. Eceiza,
385 Flexible polyurethane foam nanocomposites with modified layered hydroxides, *Appl. Clay Sci.*
386 123 (2016) 109-120, <https://doi.org/10.1016/j.clay.2016.01.015>

387 [6] K. Chen, C. Tian, S. Liang, X. Zhao, X. Wang, Effect of stoichiometry on the thermal stability
388 and flame retardation of polyisocyanurate foams modified with epoxy resin, *Polym. Degrad.*
389 *Stabil.* 150 (2018) 105-113, <https://doi.org/10.1016/j.polymdegradstab.2018.02.015>

- 390 [7] M. Kuranska, U. Cabulis, M. Auguscik, A. Prociak, J. Ryszkowaska, M. Kirpluks, Bio-based
391 polyurethane-polyisocyanurate composites with an intumescent flame retardant, *Polym. Degrad.*
392 *Stabil.* 127 (2016) 11-19, <https://doi.org/10.1016/j.polymdegradstab.2016.02.005>
- 393 [8] D.Y. Wang, *Novel fire-retardant polymers and composite materials* (1st ed) Woodhead
394 Publishing Series in Composite Science and Engineering, Woodhead Publishing, 2016.
- 395 [9] E. Asimakopoulou, J. Zhang, M. McKee, K. Wieczorek, A. Krawczyk, M. Andolfo, M. Scatto,
396 M. Sisani, M. Bastianini, A. Karakassides, P. Papakonstantinou, Fire Retardant Action of Layered
397 Double Hydroxides and Zirconium Phosphate Nanocomposites Fillers in Polyisocyanurate Foams.
398 *Fire Technol.* (2020), <https://doi.org/10.1007/s10694-020-00953-7>
- 399 [10] Asimakopoulou E., Zhang J., McKee M., Wieczorek K., Krawczyk A., Andolfo M., Scatto
400 M., Michele S., Bastianini M., Assessment of fire behaviour of polyisocyanurate (PIR) insulation
401 foam enhanced with lamellar inorganic smart fillers, *IOP Conf Series: Journal of Physics: Conf*
402 *Series* 1107: 032004 (2018), <https://doi:10.1088/1742-6596/1107/3/032004>
- 403 [11] L. Gao, G. Zheng, Y. Zhou, L. Hu, G. Feng, M. Zhang, Synergistic effect of expandable
404 graphite, diethyl ethylphosphonate and organically-modified layered double hydroxide on flame
405 retardancy and fire behavior of polyisocyanurate-polyurethane foam nanocomposite, *Polym.*
406 *Degrad. Stabil.* 101 (2014) 92-101, <https://doi.org/10.1016/j.polymdegradstab.2013.12.025>
- 407 [12] Y. Liu, Y. Gao, Q. Wang, W. Li n, The synergistic effect of layered double hydroxides with
408 other flame-retardant additives for polymer nanocomposites: a critical review, *Dalton Trans.* 47
409 (2018) 14827-14840, <https://doi.org/10.1039/c8dt02949k>
- 410 [13] C. X. Zhao, Y. Liu, D. Y. Wang, D. L. Wang and Y. Z. Wang, Synergistic effect of ammonium
411 polyphosphate and layered double hydroxide on flame retardant properties of poly(vinyl alcohol),
412 *Polym. Degrad. Stab.* 93 (2008) 1323-1331, <https://doi.org/10.1016/j.polymdegradstab.2008.04.0>
413 02

- 414 [14] C. X. Zhao, G. Peng, B. L. Liu and Z. W. Jiang, Synergistic effect of organically modified
415 layered double hydroxide on thermal and flame-retardant properties of poly(butyl acrylate-vinyl
416 acetate), *J. Polym. Res.* 18 (2011) 1971–1981, <https://doi.org/10.1007/s10965-011-9604-8>
- 417 [15] P. Ding, S. F. Tang, H. Yang and L. Y. Shi, PP/LDH nano-composites via melt-intercalation:
418 synergistic flame retardant effects, properties and applications in automobile industries, *Adv.*
419 *Mater. Res.* 87–88 (2009) 427–432, <https://doi.org/10.4028/www.scientific.net/AMR.87-88.427>
- 420 [16] L. C. Du, Y. C. Zhang, X. Y. Yuan and J. Y. Chen, Combustion characteristics and synergistic
421 effect of halogen-free flame-retarded EVA/hydrotalcite blends with expandable graphite and
422 fumed silica, *Polym. Plast. Technol. Eng.* 48 (2009) 1002–1007, [https://doi.org/10.1080/036025](https://doi.org/10.1080/03602550903092500)
423 5090 3092500
- 424 [17] X. Y. Pang, Y. Tian and X. Z. Shi, Synergism between hydro-talcite and silicate-modified
425 expandable graphite on ethylene vinyl acetate copolymer combustion behavior, *J. Appl. Polym.*
426 *Sci.* 134 (2017) 44634, <https://doi.org/10.1002/app.44634>
- 427 [18] X.M. Hu, D.M. Wang, Enhanced fire behavior of rigid polyurethane foam by intumescent
428 flame retardants, *J. Appl. Polym. Sci.* 129 (2013) 238-246, <https://doi.org/10.1002/app.38722>
- 429 [19] X. Meng, L. Ye, X. Zhang, P. Tang, J. Tang, X. Ji, Z. Li, Effects of expandable graphite and
430 ammonium polyphosphate on the flame retardant and mechanical properties of rigid polyurethane
431 foams, *J. Appl. Polym. Sc.* 114 (2009) 853-863, <https://doi.org/10.1002/app.30485>
- 432 [20] M. Kirpluks, U. Cabulis, V. Zeltins, L. Stienra, A. Avots, Rigid polyurethane foam thermal
433 insulation protected with mineral intumescent mat, *Autex Research Journal* 14 (2014) 259-269,
434 <https://doi.org/10.2478/aut-2014-0026>
- 435 [21] M. Modesti, A. Lorenzetti, Flame retardancy of polyisocyanurate–polyurethane foams: use
436 of different charring agents, *Polym. Degrad. Stabil.* 78 (2002) 341-347,
437 [https://doi.org/10.1016/S0141-3910\(02\)00184-2](https://doi.org/10.1016/S0141-3910(02)00184-2)

- 438 [22] G. Camino, S. Duquesne, R. Delobel, B. Eling, C. Lindsay, T. Roels, In: G.L. Nelson, C.A.
439 Wilkie, editors. Symposium Series No797/ Fires and Polymers. Materials and Solutions for Hazard
440 Prevention. Washington DC: ACS Pub., 2001, p 90/109.
- 441 [23] M. Thirumal, D. Khastgir, N. K. Singha, B. S. Manjunath, Y. P. Naik, Effect of Expandable
442 Graphite on the properties of intumescent flame-retardant polyurethane foam, J. Appl. Polym. Sci.
443 108 (2008) 2586, <https://doi.org/10.1002/app.28763>
- 444 [24] ISO 5660-1, Reaction to fire tests – Heat release, smoke production and mass loss rate – Part
445 1: Heat release rate (cone calorimeter method), International Organization for Standardization,
446 Geneva, Switzerland, 2002.
- 447 [25] British Standards Institution (1989) 476-6: Fire tests on building materials and structures -
448 Method of test for fire propagation for products.
- 449 [26] British Standards Institution (1997) 476-7: Fire Tests on Building Materials and Structures -
450 Method of test to determine the classification of the surface spread of flame of products.
- 451 [27] ISO 554, Standard atmospheres for conditioning and/or testing specifications, International
452 Organization for Standardization, Geneva, Switzerland, 1974.
- 453 [28] ISO 5660-1 (2002) Reaction to fire tests – Heat release, smoke production and mass loss rate
454 – Part 1: Heat release rate (cone calorimeter method), International Organization for
455 Standardization, Geneva, Switzerland.
- 456 [29] ISO 22007-2 (2015) Plastics – Determination of thermal conductivity and thermal diffusivity
457 – Part 2: Transient plane heat source (hot disk) method, International Organization for
458 Standardization, Geneva, Switzerland.
- 459 [30] C. Nyambo, E. Kandare, D. Wang, C. Wilkie, Flame-retarder polystyrene: Investigating
460 chemical interactions between ammonium polyphosphate and MgAl layered double hydroxide,
461 Polym, Degrad. Stab. 93 (2008) 1656-1663, <https://doi.org/10.1016/j.polymdegradstab.2008.05.0>
462 29

- 463 [31] J.O. Hidalgo, J.L. Torero, S. Welch, Experimental characterization of the fire behaviour of
464 thermal insulation materials for a performance-based design methodology, *Fire Technol.* (2017)
465 1201-1232, <https://doi.org/10.1007/s10694-016-0625-z>
- 466 [32] D.K. Chattopadhyay, D.C. Webster, Thermal stability and flame retardancy of polyurethanes,
467 *Progr. Polym. Sci.* (2009) 1008-1133, <https://doi.org/10.1016/j.progpolymsci.2009.06.002>
- 468 [33] L. Jial, H. Xiao, Q. Wang, J. Sun, Thermal degradation characteristics of rigid polyurethane
469 foam and volatile products analysis with TG-FTIR-MS, *Polym. Degrad. Stab.* 98 (2013) 2687-
470 2696, <https://doi.org/10.1016/j.polymdegradstab.2013.09.032>
- 471 [34] B. K. Kandola, R. A. Horrocks, P. Myler, D. Blair, New developments in flame retardancy of
472 glass-reinforced epoxy composites, *J. Appl. Polym. Sci.* 88 (2003) 2511-21,
473 <https://doi.org/10.1002/app.11909>
- 474 [35] B. K. Kandola, S. Horrocks, R. A. Horrocks, Evidence of interaction in flame-retardant fibre-
475 intumescent combinations by thermal analytical techniques, *Thermochim. Acta* 294 (1997)113-
476 25, [https://doi.org/10.1016/S0040-6031\(96\)03151-6](https://doi.org/10.1016/S0040-6031(96)03151-6)
- 477 [36] J. Xu, T. Wu, C. Peng, S. Adegbite, Influence of acid and alkali pre-treatments on thermal
478 degradation behaviour of polyisocyanurate foam and its carbon morphology, *Polym. Degrad.*
479 *Stabil.* 141 (2017) 104-118, <https://doi.org/10.1016/j.polymdegradstab.2017.05.018>
- 480 [37] X. Shi, S. Jiang, J. Zhu, G. Li, X. Peng, Establishment of a highly efficient flame-retardant
481 system for rigid polyurethane foams based on bi-phase flame-retardant actions, *RCS Adv.*, 8
482 (2018) 9985-9995, <https://doi.org/10.1039/C7RA13315D>
- 483 [38] K.S. Lim, S.T. Bee, L.T. Sin, T.T. Tee, C.T. Ratnam, D. Hui, A.R. Rahmat, A. R., A review
484 of application of ammonium polyphosphate as intumescent flame retardant in thermoplastic
485 composites, *Compos. Part B-Eng.* 84 (2016) 155-174,
486 <https://doi.org/10.1016/j.compositesb.2015.08.066>
- 487 [39] F. Tuinstra and J. L. Koenig., Raman Spectrum of Graphite, *J. Chem. Phys.* 53 (1970) 1126-
488 1130, <https://doi.org/10.1063/1.1674108>

489 **FIGURE CAPTIONS**

490

491 Figure 1: Morphological evaluation using optical microscopy (500 μm scale) of REF (a) and PL
492 (b) samples.

493

494 Figure 2: SEM images (500 μm scale) of PLE (a), PLEAPP1 (b), PLEAPP2 (c) samples.

495

496 Figure 3: TGA (left) and DTGA (right) of all the formulations in N_2 atmosphere.

497

498 Figure 4: TGA (left) and DTGA (right) of all the formulations in air atmosphere.

499

500 Figure 5: Real time FTIR spectra of (a) and (f) REF, (b) and (g) PL, (c) and (h) PLE, (d) and (i)
501 PLEAPP1, (e) and (j) PLEAPP2 samples, in N_2 (a)-(e), and air, (f)-(j) atmosphere.

502

503 Figure 6: Temporal absorbance of pyrolysis products of all samples: (a) ethers (1133 cm^{-1}), (b)
504 NCO (2279 cm^{-1}), (c) CO (2181 cm^{-1}), (d) CO_2 (2352 cm^{-1}) samples under air atmosphere.

505

506 Figure 7: Comparisons of HRR at 20 kW/m^2 (left) and 50 kW/m^2 (right) of all formulations.

507

508 Figure 8: Comparisons of SPR at 20 kW/m^2 (left) and 50 kW/m^2 (right) of all formulations.

509 Figure 9: Digital photos of charred samples of (a) and (f) REF, (b) and (g) PL, (c) and (h) PLE,
510 (d) and (i) PLEAPP1, (e) and (j) PLEAPP2 after CC testing at 20 kW/m^2 , (a)-(e), and 50
511 kW/m^2 , (f)-(j).

512

513 Figure 10: SEM images of (a)-(c) REF, (d)-(f) PL, (g)-(i) PLE, (j)-(l) PLEAPP1 and (m)-(o)
514 PLEAPP2 charred samples.

515

516 Figure 11: Raman spectra for a) PLE, b) PLEAPP1 and c) PLEAPP2 samples. D, G and 2D
517 represent the characteristic bands of expandable graphite.

518

519 Figure 12: Diagrammatic illustration of the flame-retardant mechanism of LDH, EG and APP
520 additives in PIR samples.

521

522 **TABLES CAPTIONS**

523

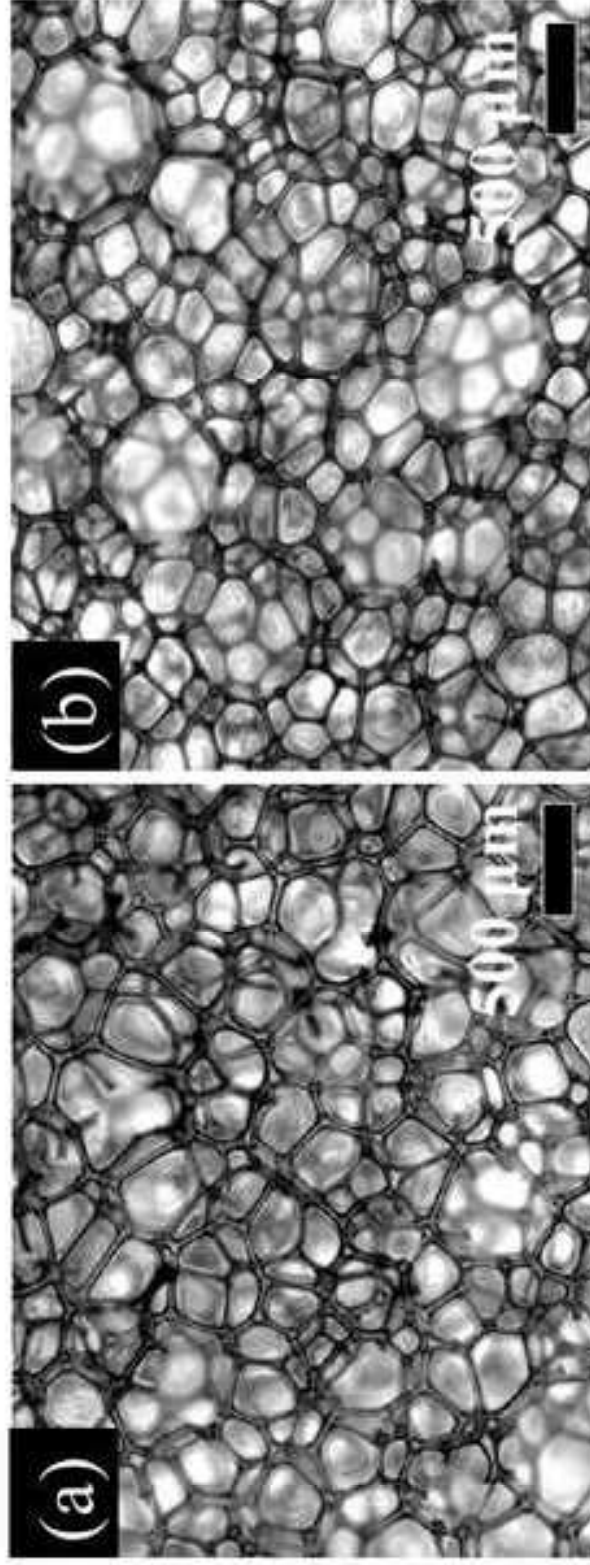
524 Table 1. Samples composition, physical and mechanical characteristics.

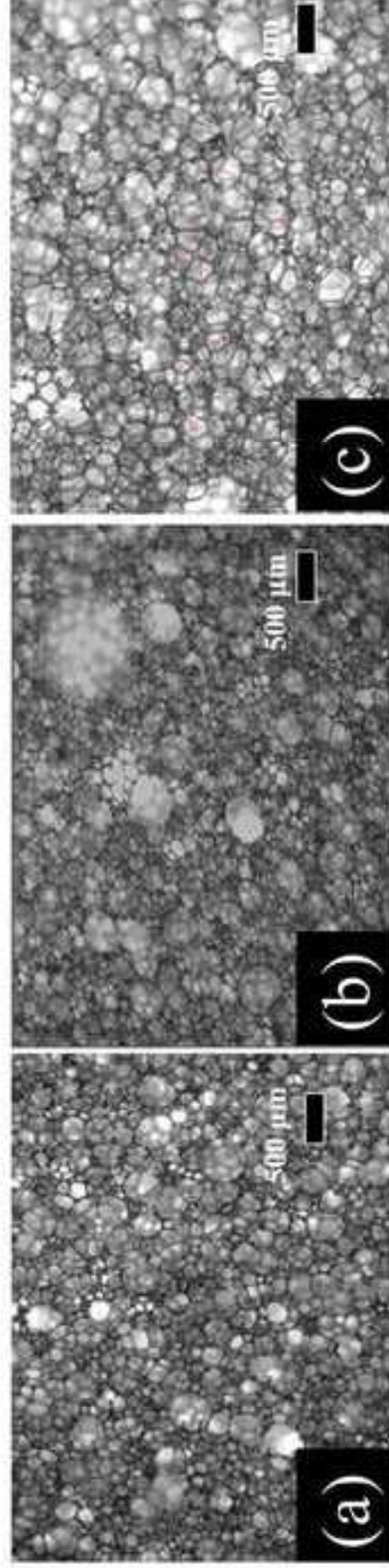
525

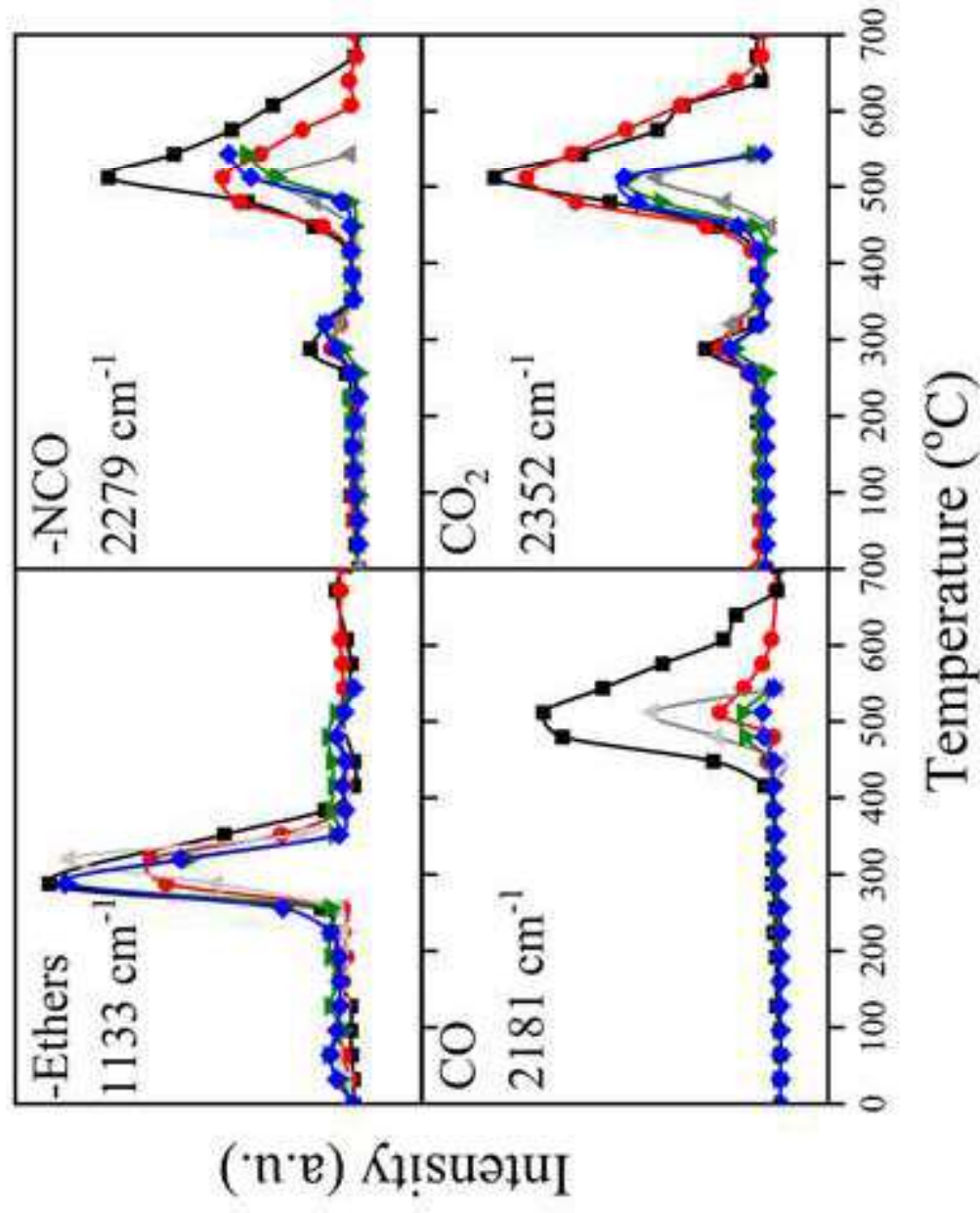
526 Table 2. TG/DTG results of all formulations.

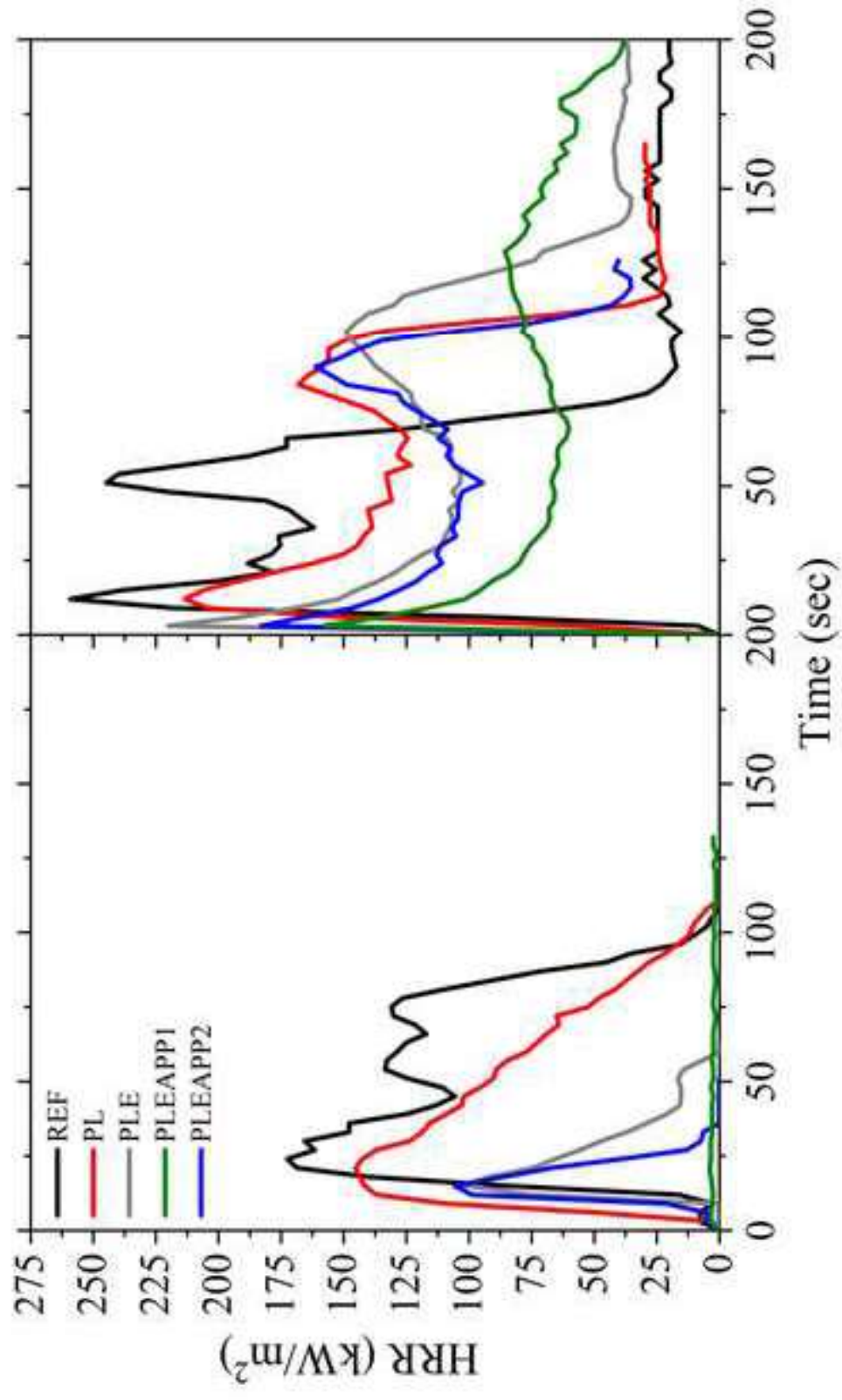
527

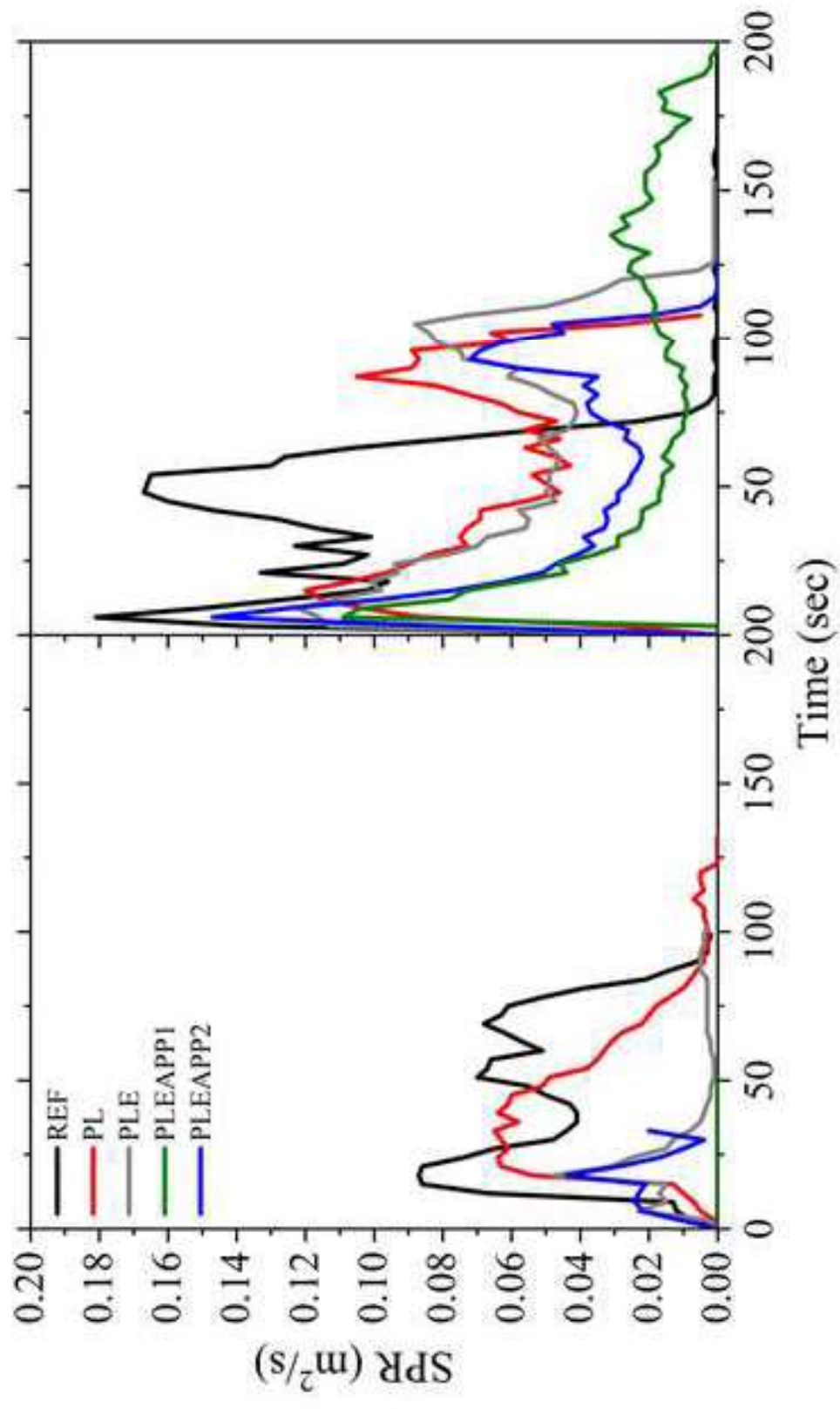
528 Table 3. Cone calorimetry data for PIR samples at 20 kW/m² and 50 kW/m².

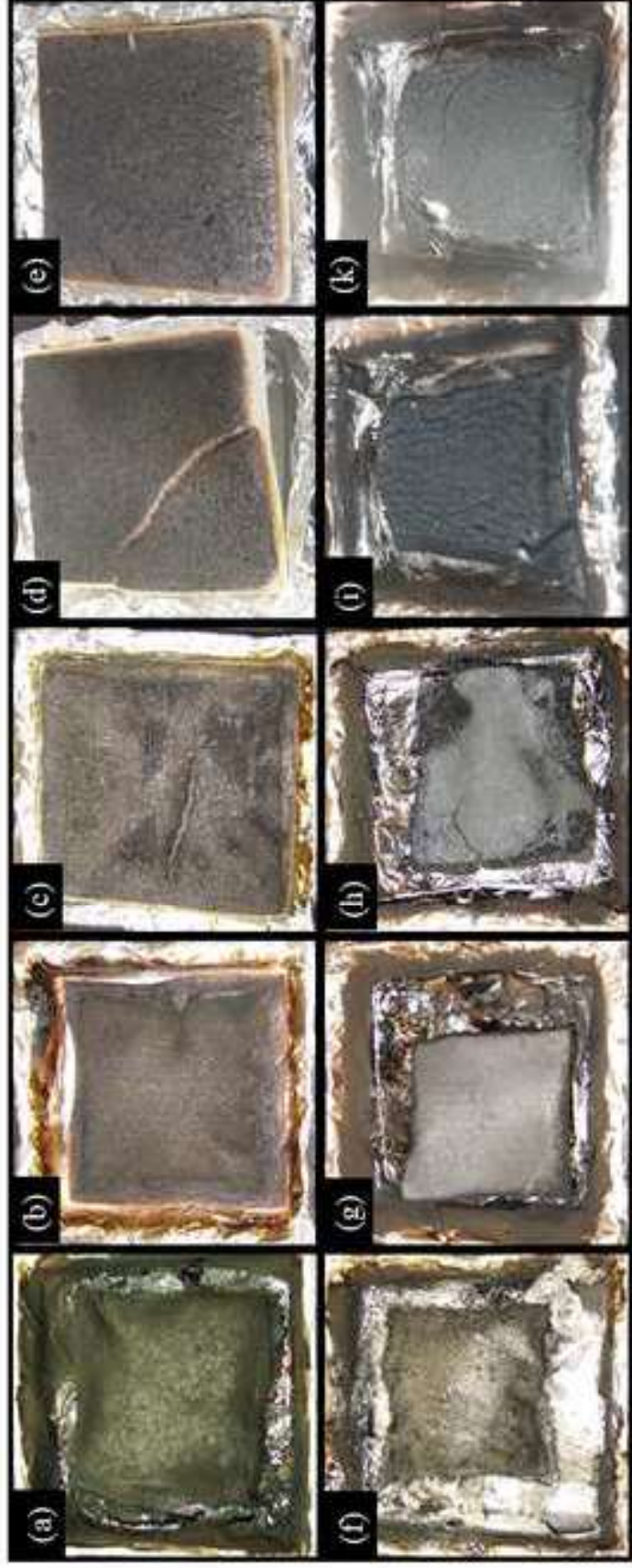


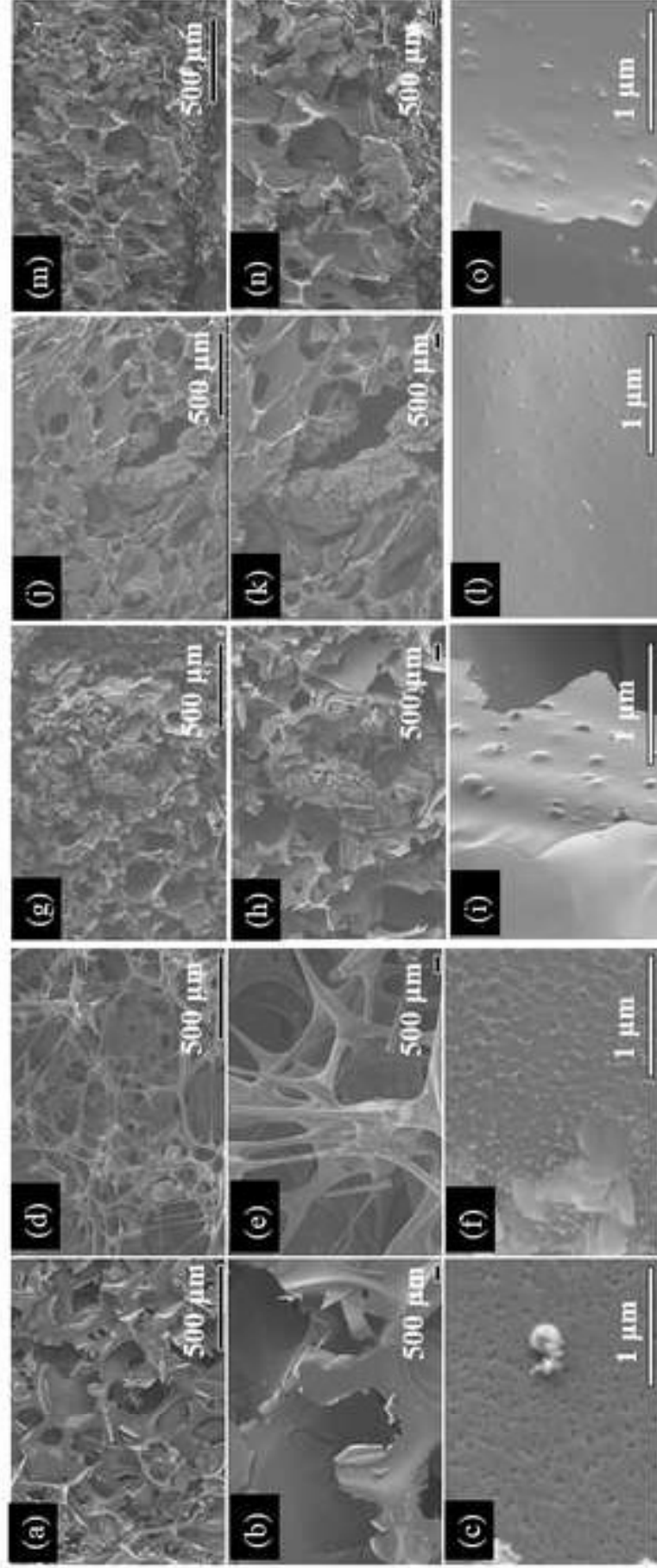


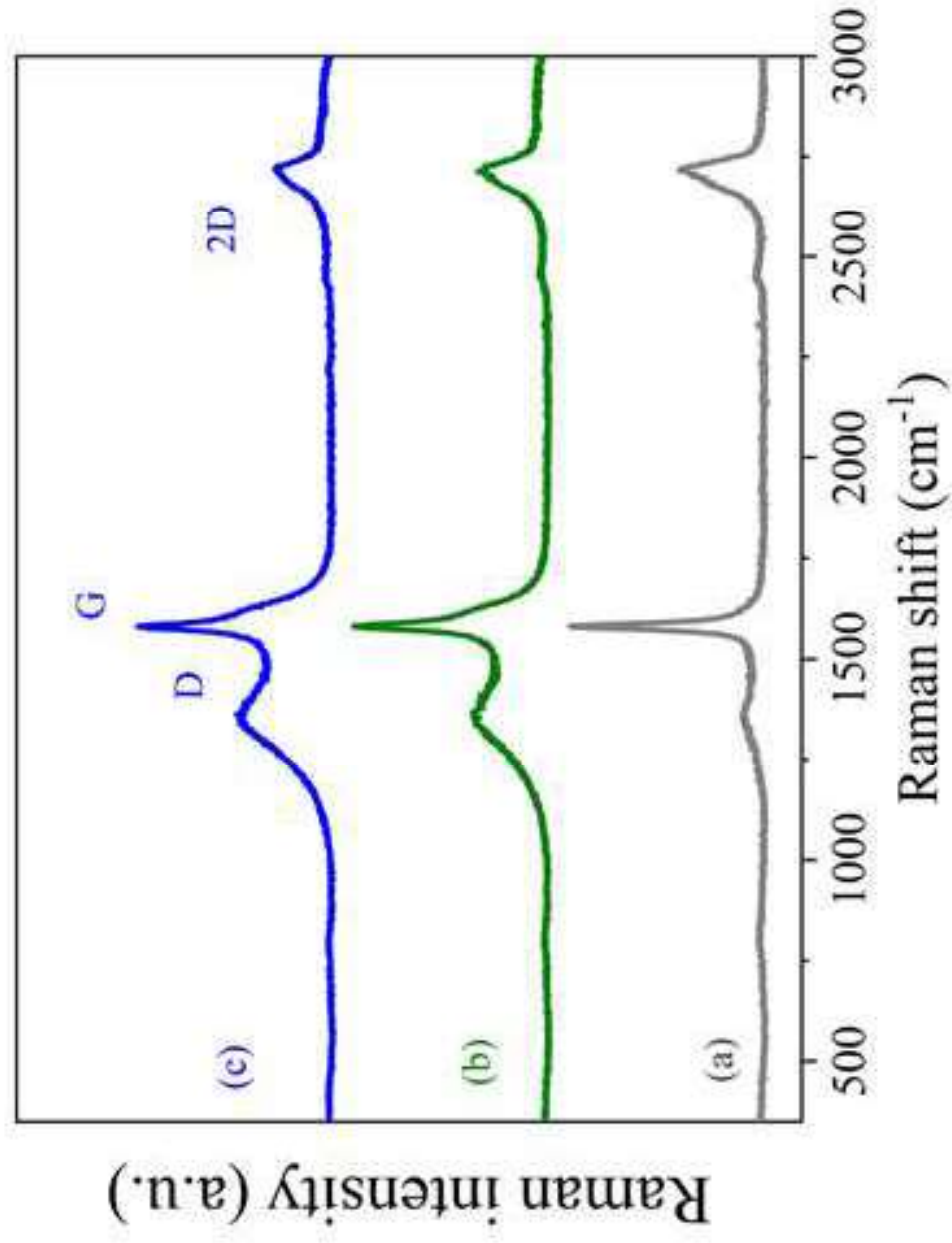


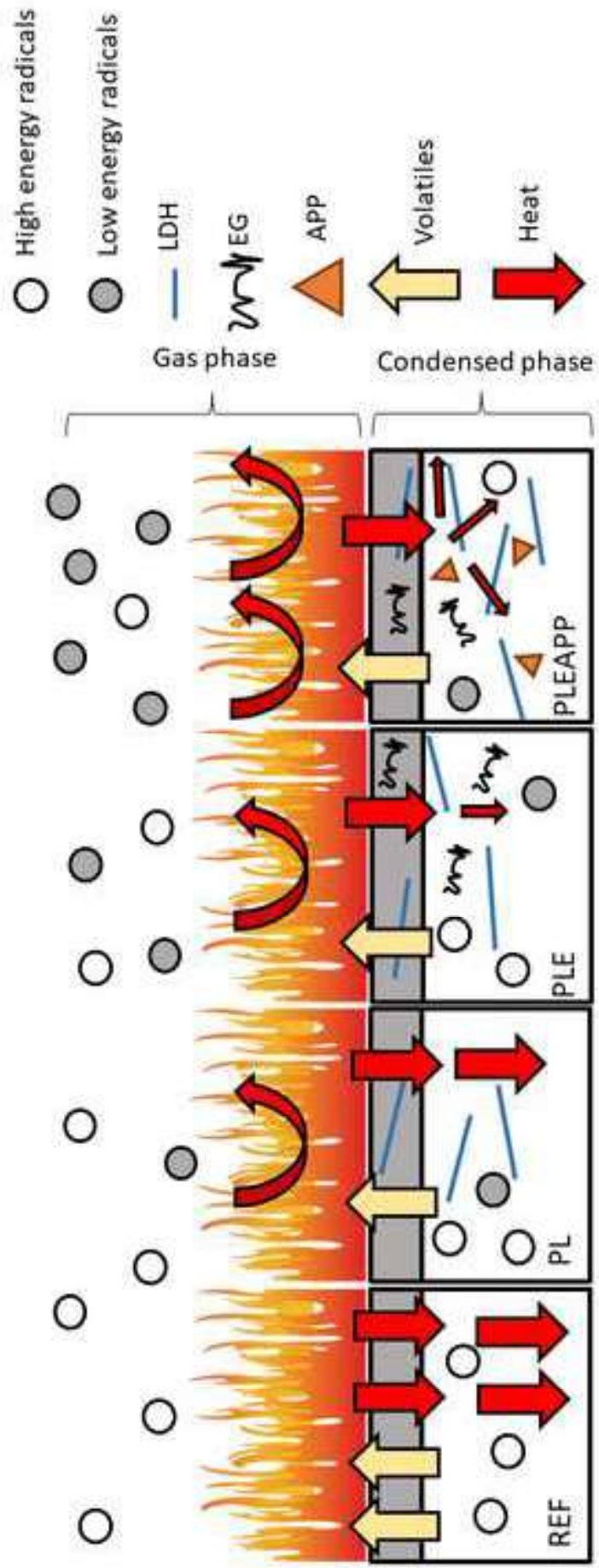


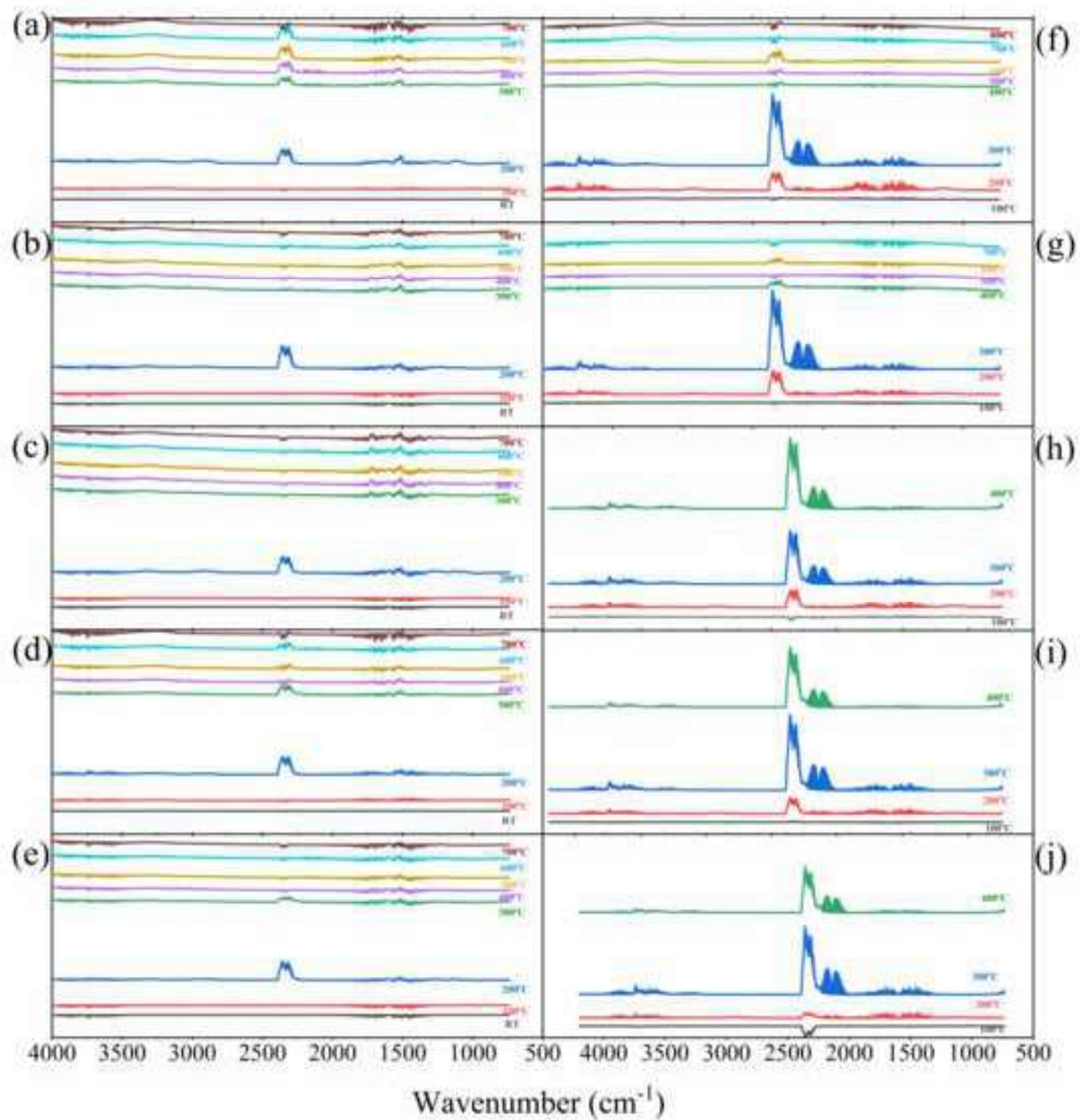


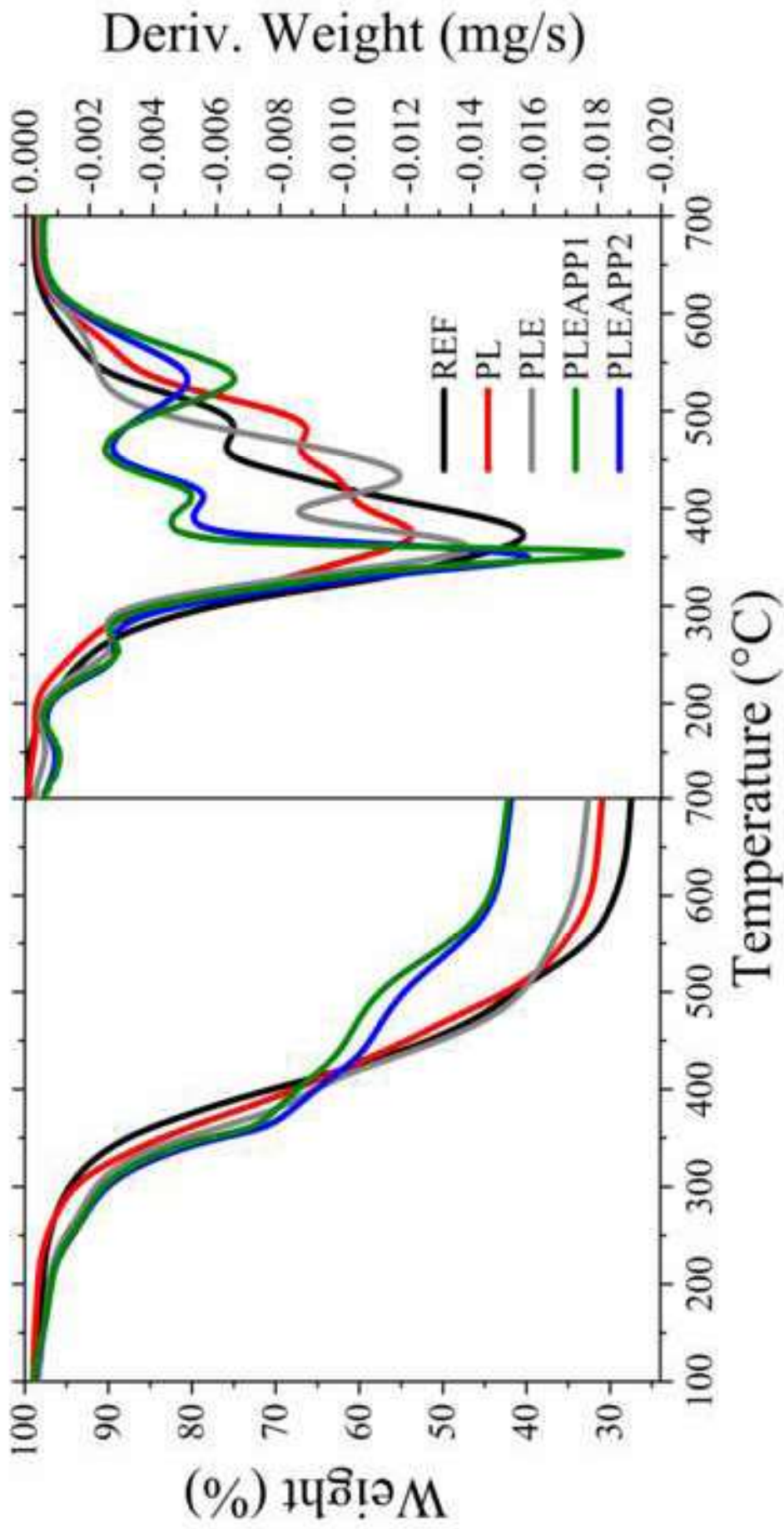


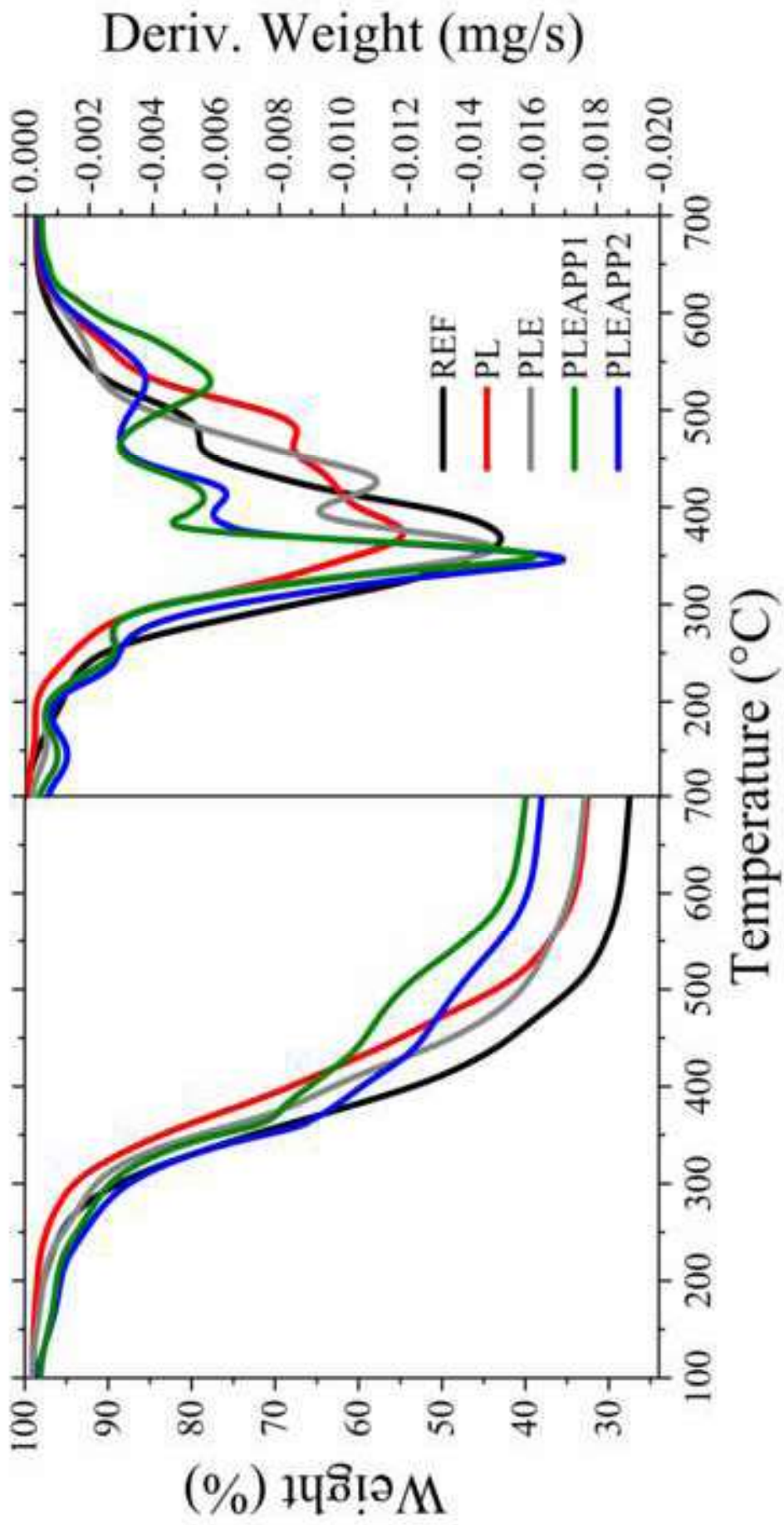






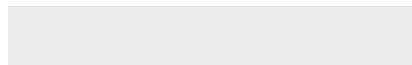
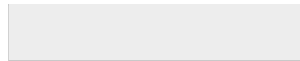






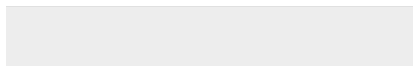
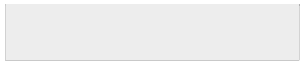


Click here to access/download
Table
Table1_revised.docx





Click here to access/download
Table
Table2_revised.docx





Click here to access/download
Table
Table3_revised.docx

